Inflight Performance of the TanSat Atmospheric Carbon Dioxide Grating Spectrometer

Zhongdong Yang, Yan-Meng Bi, Qian Wang, Cheng-Bao Liu, Song-Yan Gu, Yuquan Zheng, Chao Lin, Zengshan Yin, and Longfei Tian

***Abstract*— TanSat was successfully launched on December 22, 2016, and has been acquiring global measurements of CO_2 and O_2 spectral bands in reflected sunlight since early February 2017. The atmospheric carbon dioxide grating spectrometer (ACGS) is a spaceborne three-band grating hyperspectral spectrometer suite onboard TanSat. The ACGS is designed to measure high-spectral-resolution, coboresighted spectra of reflected sunlight within the molecular oxygen (O_2) A-band range from 0.758 to 0.778 μm and the weak and strong absorption bands of carbon dioxide (WCO_2 and SCO_2) ranging from 1.594 to 1.624 μm and from 2.042 to 2.082 μm, respectively. The spectral resolving power ($\lambda/\Delta\lambda$) of the ACGS is $\sim$19 000, $\sim$12 800 and $\sim$12 250 in the O_2 A-band, WCO_2 band and SCO_2 band, respectively. The inflight radiometric calibration accuracy is better than 5%, which satisfies the required specification. The wavelength calibration accuracy of the O_2 A-band is $\sim$0.19 pm, that of the WCO_2 band is $\sim$0.27 pm, and that of the SCO_2 band is $\sim$4.75 pm, all of which meet the 0.05 full-width at half-maximum (FWHM) requirement. The spectroscopic performance of the ACGS exceeds the mission requirements by a margin. The ACGS has noise levels that are comparable to or smaller than those observed during prelaunch testing, and the noise has remained stable in the three bands during inflight operations. The signal-to-noise ratio (SNR) levels of the three bands meet the specified requirements. As expected, the ACGS radiometric performance in the O_2 A, WCO_2, and SCO_2 bands was fairly good during its first 17 months inflight.**

***Index Terms*— Atmosphere, carbon dioxide, sounding, spectrometer.**

I. Introduction

THE latest scientific assessment by the Intergovernmental Panel on Climate Change indicates that climate warming is unequivocal. Many of the observed changes in recent years are unprecedented over timescales spanning decades to millennia. The atmosphere and ocean have warmed, snow and ice have diminished, and sea levels have risen. Such changes have resulted from positive radiative forcing caused by increased concentrations of atmospheric greenhouse gases. Among these gases, carbon dioxide (CO_2) is the largest contributor to this radiative forcing [1].

The concentrations of atmospheric carbon dioxide increased very rapidly to above 403 ppm in 2016 to the highest level in 800 000 years according to the World Meteorological Organization's Greenhouse Gas Bulletin [1]. These abrupt changes in the atmosphere witnessed over the past 70 years are without precedent. As a result of the combination of human activities and a strong El Nino event, the globally averaged concentration of CO_2 reached 403.3 parts per million in 2016 (up from 400.0 ppm in 2015). The concentrations of CO_2 are now 145% of preindustrial (before 1750) levels according to the Greenhouse Gas Bulletin [1].

Reliable predictions of future levels of atmospheric CO_2 require a quantitative understanding of both CO_2 emissions and the specific processes and reservoirs responsible for sequestering CO_2. Although atmospheric CO_2 concentration measurements from surface networks are highly accurate, such networks are too sparse to adequately characterize both the geographical distribution of CO_2 sinks and the processes controlling their variability. However, space-based sensors can acquire atmospheric CO_2 measurements at suitable spatial and temporal scales.

In recent decades, several satellites have been launched into low Earth orbit. In March 2002, the Scanning Imaging Absorption Spectrometer for Atmospheric Chartography (SCIAMACHY) atmospheric science instrument, which was launched onboard the European Space Agency's (ESA's) Environmental Satellite (ENVISAT) mission into low Earth orbit, became the first imaging absorption grating spectrometer that operates in the visual and near-infrared spectral range and addresses the need to both improve our understanding of biogeochemical cycling and assess the impacts of humans on the Earth system [2]. SCIAMACHY measurements aim to provide the distributions of several important greenhouse gases (CO_2, H_2O, and CH_4) and aerosols in addition to cloud data. The Orbiting Carbon Observatory-2 (OCO-2) was the first satellite designed by the National Aeronautics and Space Administration (NASA) that is dedicated to measuring atmospheric CO_2 concentrations with accuracy, resolution, and coverage needed to quantify CO_2 fluxes on regional scales [3]. OCO-2 was

Manuscript received July 20, 2018; revised February 17, 2019, July 26, 2019, and November 19, 2019; accepted January 8, 2020. Date of publication January 29, 2020; date of current version June 24, 2020. This work was supported by the Ministry of Science and Technology (MOST) of the China Earth Observation Program under Contract 2011AA12A104. *(Corresponding author: Zhongdong Yang.)*

Zhongdong Yang, Yan-Meng Bi, Qian Wang, Cheng-Bao Liu, and Song-Yan Gu are with the National Satellite Meteorological Centre (NSMC), Beijing 100081, China (e-mail: yangzd@cma.cn).

Yuquan Zheng and Chao Lin are with the Changchun Institute of Optics, Fine Mechanics and Physics (CIOFMP), Chinese Academy of Sciences (CAS), Changchun 130033, China.

Zengshan Yin and Longfei Tian are with the Shanghai Engineering Centre for Microsatellites (SECM), Chinese Academy of Sciences (CAS), Shanghai 201203, China.

Color versions of one or more of the figures in this article are available online at http://ieeexplore.ieee.org.

Digital Object Identifier 10.1109/TGRS.2020.2966113

successfully launched on July 2, 2014, and since then, it has collected data of more than five years of observation [4]. The Greenhouse Gases Observing Satellite (GOSAT) was developed by the Japan Aerospace Exploration Agency (JAXA) to provide independent measurements of the global distributions of atmospheric CO_2 from space. GOSAT, a Fourier transform spectrometer with a completely different technical system, was successfully launched on January 23, 2009 [5]. Nevertheless, although these satellites have obtained many important space-based measurements of atmospheric CO_2, improvements in the sensitivity and sustainability of their observations are necessary.

TanSat is the first Chinese satellite mission dedicated to measuring the column-averaged CO_2 dry-air mole fraction (X_{CO_2}); for this purpose, TanSat is equipped with the atmospheric carbon dioxide grating spectrometer (ACGS), a major spaceborne grating hyperspectral spectrometer suite. TanSat was successfully launched into orbit from JiuQuan Base in Gansu Province, China, on December 22, 2016. TanSat orbits at an altitude of 700 km above the Earth's surface with an inclination angle of 98.25° and a 13:45 local time ascending node. The ACGS has been providing global measurements of CO_2 and O_2 spectral bands in reflected sunlight since early February 2017.

The ACGS is a three-band, high-spectral-resolution grating spectrometer on the TanSat satellite that provides high-resolution measurements of top-of-atmosphere visible and near-infrared radiance spectra; these measurements are used for climate research and as inputs for chemistry transport models for investigating carbon sources and sinks at both the regional and global scales [6]. This instrument represents a major step forward in the Chinese scientific space-based measuring capability of atmospheric CO_2, which was previously provided by the American OCO-2 and Japanese GOSAT satellites. The ACGS has a high spectral resolution, a large number of channels, a high signal-to-noise ratio (SNR), and a high dynamic range, all of which collectively result in a substantially improved resolution, accuracy, and sampling rate relative to GOSAT. Following OCO-2, the ACGS is the second grating spectrometer dedicated to measuring atmospheric CO_2 concentrations. However, while the ACGS has a spectral coverage similar to that of OCO-2 and achieves a similar spectral resolution in the O_2 A-band, the ACGS has only two-thirds the spectral resolution of OCO-2 in the CO_2 bands. Hence, ACGS has the ability to enrich the measurements provided by OCO-2.

The ACGS measurements are calibrated and geolocated to produce level 1 (L1) products that are analyzed to retrieve spatially resolved estimates of X_{CO_2}. The spatial and temporal variations in X_{CO_2} are then analyzed in the context of an atmospheric chemistry transport model to quantify the surface sources and sinks of CO_2 [6], [7]. According to a geostatistical study, the largest emission sources and natural absorbers of CO_2 produce only very small ($\sim$0.25%) variations in the background X_{CO_2} field over spatial scales ranging from a few square kilometers to the continental scale, which constitutes a rigorous challenge for space-based measurements [8]. To apply ACGS data to chemistry transport models needed to perform investigations of carbon sources and sinks and of climate change similar to those explored with OCO-2 data [3], [9], [10], it is important for the radiometric and spectroscopic accuracies of the ACGS to be meticulously validated. These demanding applications represent the motivation for the characterization of the ACGS radiometric and spectroscopic accuracies provided in this article. In addition to understanding the physical basis of the uncertainties in the ACGS measurements, it should be possible to achieve even higher accuracies in space-based atmospheric CO_2 measurements in the near future. Since TanSat was launched in 2016, a team of subject matter experts from the government, academic, and industrial sectors has been engaged in the inflight TanSat testing, which includes ACGS calibration and validation activities; this inflight check was completed in September 2017.

In this article, we present the inflight performance of the ACGS during the first 17 months after TanSat was launched. The ACGS calibration process includes both prelaunch and inflight activities performed by a team consisting of subject matter experts from academia, operations, and industry. Their prelaunch calibration work successfully established the baseline instrument characterization and performance, as well as the initial set of instrument calibration coefficients and parameters for the processing of L1 products [11], [12]. The inflight performance and absolute accuracy of any sounding instrument are based on the basic design, ground-based calibration, and inflight refinement of the calibration parameters. The inflight calibration objectives are to safely and effectively configure the ACGS for operational conditions, verify the L1 products, examine the functionality of the instrument, optimize the instrument settings, refine the ACGS preprocessing algorithm, tune the calibration parameters, and validate the ACGS L1 products. At the time of this writing, the inflight calibration of the ACGS has achieved success, that is, the radiometric and spectral performance specifications have been met. In this article, we describe the ACGS measurement characteristics and inflight calibration device in Section II. Section III demonstrates the inflight spectroscopic and radiometric performance of the ACGS, Section IV provides results and discussion, and Section V presents the conclusions of this article.

II. Major Instrument of TanSat: ACGS

The TanSat platform carries two instruments. The first is the main instrument, the ACGS, and the other is a visible and near-infrared spectra cloud and aerosol polarization imager (CAPI). This article focuses on the ACGS.

A. Performance Specifications

The ACGS is a three-band atmospheric CO_2 grating high-resolution spectrometer designed to measure superresolution, coboresighted spectra of reflected sunlight within the molecular oxygen (O_2) A-band range from 0.758 to 0.778 μm; the weak carbon dioxide (WCO_2) absorption band range from 1.594 to 1.624 μm; and the strong carbon dioxide (SCO_2) range from 2.042 to 2.082 μm. The spectral resolving power of the ACGS ($\lambda/\Delta\lambda$) is $\sim$19 000, $\sim$12 800, and $\sim$12 250 in the O_2 A-band, WCO_2 band, and SCO_2 band, respectively.

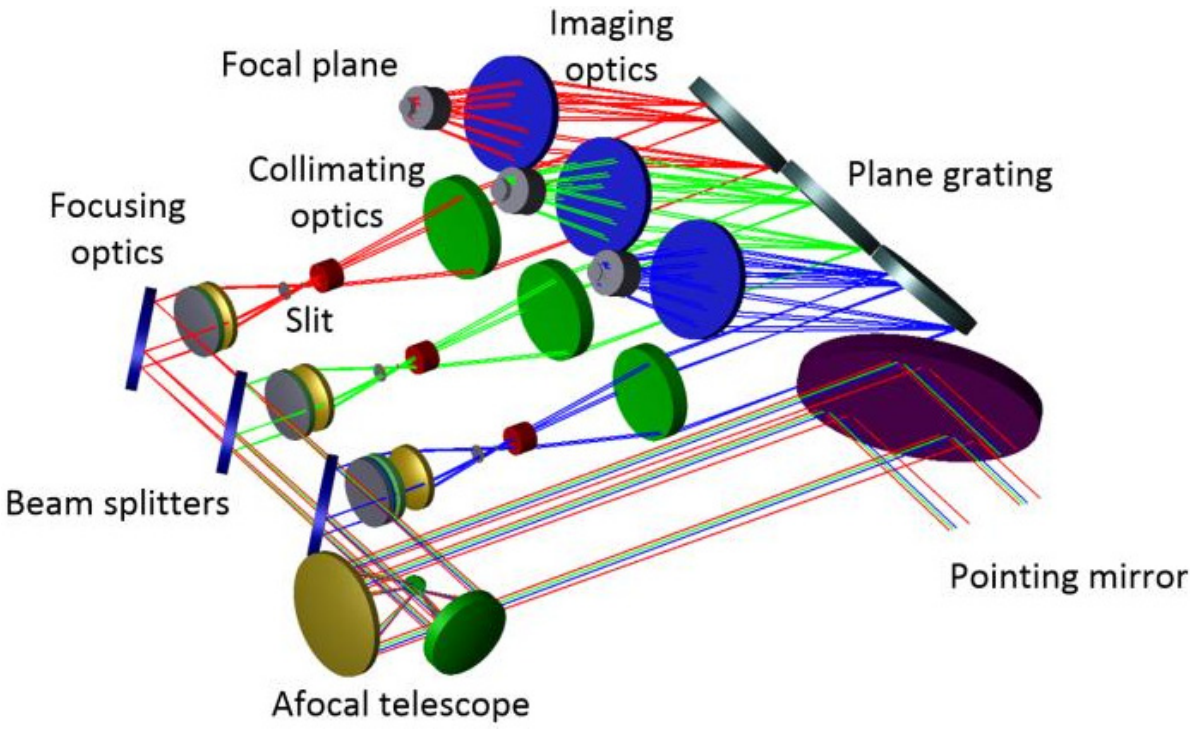

Fig. 1. Optical layout of the TanSat ACGS.

TABLE I
PERFORMANCE REQUIREMENTS OF THE ACGS

Item \ Band	O_2A	WCO_2	SCO_2
Spectral Range (nm)	758 - 778	1594 - 1624	2042 - 2082
Spectral Resolution (nm)	0.033 - 0.047	0.120 - 0.142	0.160 - 0.182
Spectral Resolving ($\lambda/\Delta\lambda$)	~19000	~12800	~12250
Spectral Sampling Per FWHM	>2		
Dynamic Range ($ph/sec/m^2/sr/um$)	SNR=1@$1.2\times10^{17}\sim1.4\times10^{21}$	SNR=1@$5.7\times10^{16}\sim4.9\times10^{20}$	SNR=1@$6.0\times10^{16}\sim1.6\times^{20}$
SNR @ ($ph/sec/m^2/sr/um$)	360@5.8×10^{19}	250@2.1×10^{19}	180@1.1×10^{19}
Abs/Rel Calibration Error (%)	<5 / <3		
Calibration Nonlinearity Error (%)	<2		
Dark Current Error (DNs) (after correction)	<5		
Radiance Response Uniformity (%) (interior of band)	>99.9		
Radiance Response Uniformity (%) (between bands)	>99.0		
Frame Rate (Hz)	~3.3		
IFOV (Km^2)	2×3		

More detailed performance specifications of the ACGS are presented in Table I, which describes all of the major spectral and radiometric performance specifications.

B. Optical System

The ACGS consists of three spectrometers targeting the O_2A, WCO_2, and SCO_2 bands. These three spectrometers are integrated into a common structure to improve the rigidity and thermal stability of the system [11]. As depicted in Fig. 1, which displays the optical layout of the ACGS, radiation originating from the Earth's atmosphere illuminates the front side of the pointing mirror of the ACGS, while the back side of the mirror is a diffuse plane used for inflight solar calibration purposes. The front side of the pointing mirror reflects atmospheric radiation into a focal telescope consisting of two paraboloidal mirrors. Then, this collimated exit radiation is directed through beam splitters, filters, polarizers, and focusing optics to concentrate the spectral radiation in each band into each slit, after which the spectral radiation through each slit is collimated on the gratings by collimating optics. Finally, the dispersed spectral radiance is recorded by each focal plane array (FPA) detector of the three spectrometers. The sampling frame frequency of each detector is 3.3 Hz. The slit, diffractive grating, and FPA are the three key components of the ACGS. The slit size of the O_2 A band is 7.5 mm $\times$ 22.5 μm, and that of the WCO_2 and SCO_2 bands is 7.5 mm $\times$ 37.5 μm. Each of the diffractive gratings has a size of 140 mm $\times$ 190 mm. The FPA size of the O_2 A band is 360 μm (spatial) $\times$ 22.5 μm (spectral), and that of the WCO_2 and SCO_2 bands is 360 μm (spatial) $\times$ 30 μm (spectral). The ACGS uses three flat holographic gratings operating in the first order. Just before the radiation enters each spectrometer, a linear polarizer selects only the polarizing vector perpendicular to the entrance slit.

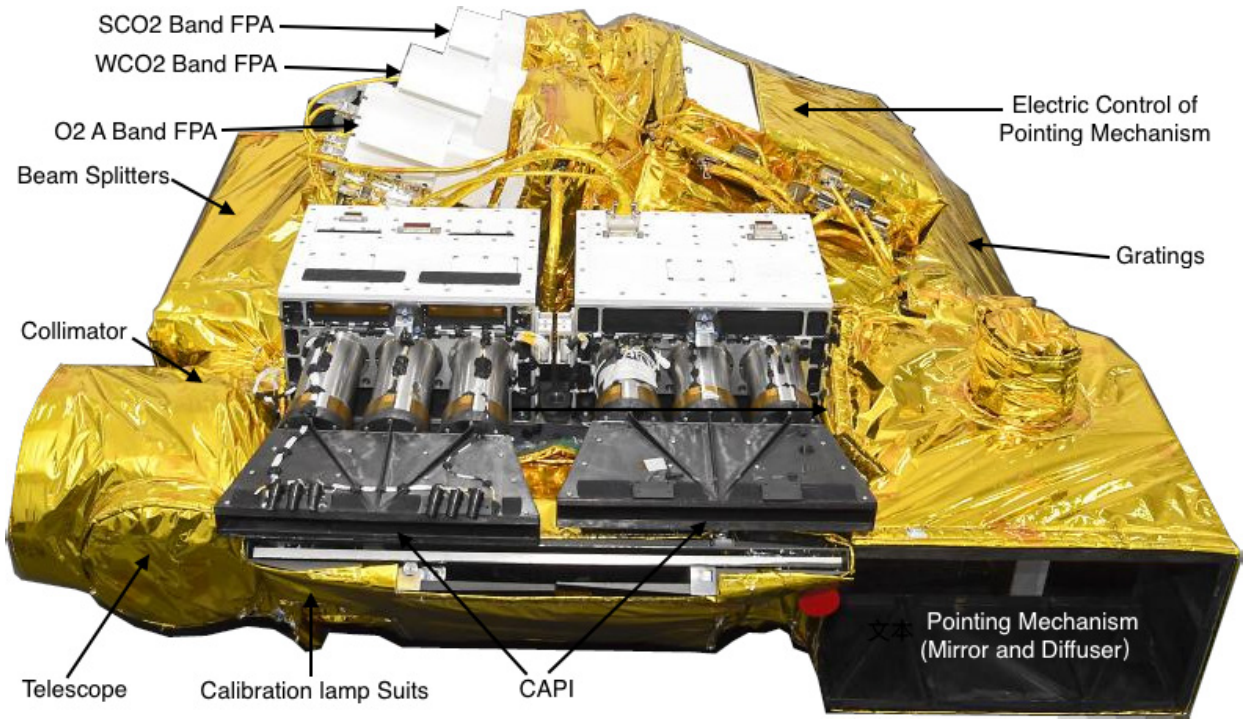

Fig. 2. Physical photograph of the inflight ACGS.

A telescope system with a focal length of 252 mm and an instantaneous field of view (IFOV) of $0.0818° \times 0.00456°$ is shared among the three spectrometers through a series of beam splitters and imaging optics. A physical photograph of the inflight ACGS is shown in Fig. 2.

Three diffractive gratings, which represent pivotal components of the ACGS, are used to disperse the spectra for each of the three spectrometers. The diffractive efficiency of each grating is above 80%, and the wavefront error is one-fourth of the wavelength. At the focus of each diffractive grating, a two-dimensional FPA detector collects the band spectral radiation; one dimension is used to record the field of view along the slit as the spatial dimension, while the other dimension measures radiation in different wavelengths as the spectral dimension. The FPA detector of the O_2 A-band consists of 1242 (spectral dimension) $\times$ 320 (spatial dimension) array elements, while the other two CO_2 FPA detectors consist of 500 (spectral dimension) $\times$ 256 (spatial dimension) array elements. In the spectral dimension, spectral sampling includes more than two elements of the FPA detector per full-width at half-maximum (FWHM) in the range of each full CO_2 absorbing band. The spectral resolving power ($\lambda/\Delta\lambda$) of the ACGS is $\sim$19 000, $\sim$12 800, and $\sim$12 250 in the O_2 A-band, WCO_2, band and SCO_2 band, respectively. In the spatial dimension, sets of 24 array elements are combined to yield 9 useful spatial footprints such that each footprint has a size of $\sim 2 \times 3$ km^2 on the ground.

C. Inflight Calibration System

There are two sets of lamp calibration devices. One is routinely used each day during the first half of the year, and the other is used only one time per half-year to check and validate the inflight stability of the ACGS. Each device consists of one halogen tungsten lamp manufactured by OSRAM. One silicon and two InGaAs detectors are used to monitor the stability of the lamp; the spectral ranges of the three monitoring detectors are similar to those of the three ACGS bands. The results from the monitoring detectors indicate that the stability of the calibration lamp is better than 0.5% per hour, and the SNR of each monitoring detector is greater than 300.

When TanSat crosses the northern terminator during every orbit, the pointing mechanism is turned from the position used to acquire scientific observations to the solar calibration position; then, the diffuser is turned toward the Sun, and the solar irradiance is recorded by the three FPA detectors of the ACGS bands. These solar calibration measurements are used to check and validate the absolute radiometric response and spectral accuracy of the ACGS. After performing solar calibration, the pointing mechanism is turned to the lamp calibration position from the solar calibration position, the routine calibration lamp is powered on, the diffuser is illuminated, and the halogen tungsten lamp irradiance is recorded by the three FPA detectors of the ACGS bands. These measurements are used to monitor the responses of the individual pixels and spectral samples. After calibrating the lamp in each orbit, the calibration lamp is powered off, and the dark current calibration is conducted.

III. Inflight Performance

The inflight performance and absolute accuracy of any remote sensing satellite instrument are based on the optimal design of the optics, electricity and thermotics systems, ground

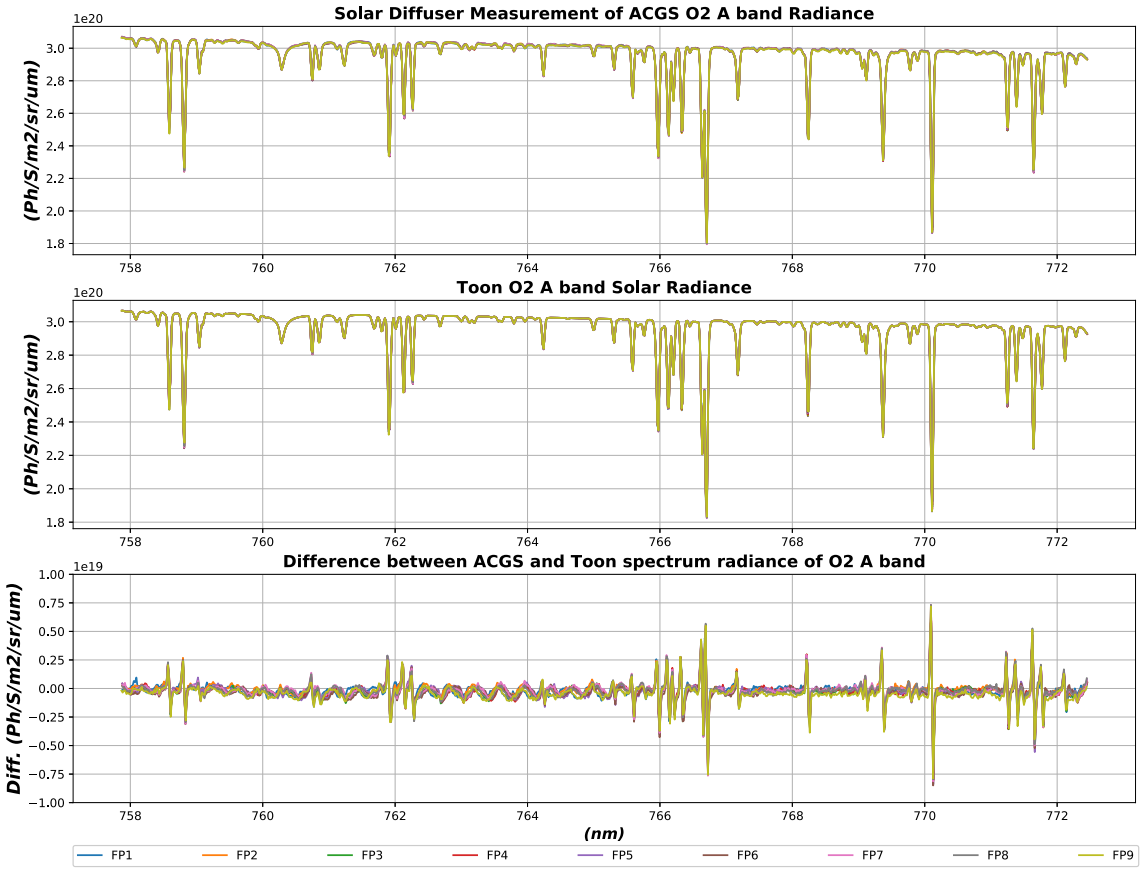

Fig. 3. Inflight spectroscopic performance of the ACGS O2 A-band in nine footprints.

laboratory calibration, and inflight refinement of the calibration parameters. The performance of the ACGS was carefully characterized and calibrated twice prior to launch, and the results met the mission requirements [11]. To date, the ACGS has performed as expected inflight. During the first month following its launch in 2016, the spacecraft team completed a functional check of the platform and instruments. At the time of this writing, the instruments and spacecraft are performing extremely well, and data collection continues.

A. Spectroscopic Performance

The instrument line shape (ILS) describes the form of the spectral response of the spectrometer, whose key parameters are the line position, maximum height, and FWHM. The ILS of the ACGS is determined by the slit width, pixel pitch, optical aberrations, diffraction, and detector crosstalk. The ILS profile and dispersion coefficient of the ACGS were carefully characterized and calibrated prior to launch [12].

Inflight, we used the available Fraunhofer lines of the solar spectra acquired during solar calibration observations of the ACGS after correcting for the Doppler effect and performed a comparison with the more precise solar spectra database used by OCO-2 as a reference to validate the spectral accuracy of the centroid wavelength [13], [14]. The selected Fraunhofer lines must have a greater depth and wider absorption to be identified by the ACGS. Figs. 3–5 show the inflight spectroscopic performance of the three bands of the ACGS; the red lines are the solar reference spectra, the black lines are the solar spectra of the nine footprints measured by the ACGS, and the bottom lines represent their differences in Figs. 3–5. These figures illustrate remarkable consistencies among the footprints and agreements with the solar reference spectra. The spectral bias of the ACGS of the O2 A-band was 2.93 pm, that of the WCO_2 band was -42.9 pm, and that of the SCO_2 band was -46.7 pm from the results of the inflight check. After a spectral bias correction, the wavelength calibration accuracy of the O_2 A-band was 0.19 pm, that of the WCO_2 band was 0.27 pm, and that of the SCO_2 band was 4.75 pm, all of which meet the 0.05 FWHM requirement. The wavelength calibration accuracy is derived from the statistical root-mean-square (rms) error in Figs. 3–5 using the Fraunhofer lines. To validate the wavelength calibration accuracy, we compare the wavelength positions of typical Fraunhofer lines in the ACGS observations to their positions in the solar reference spectra. As shown in Fig. 6, the spectral positions are stable with time, and there were only slight fluctuations (on the order of a few picometers, especially after April 2018) over the course of one year in each of the three bands. The spectroscopic performance of the ACGS, therefore, surpasses the mission requirements by a margin and has comparable or superior performance with similar instruments.

B. Radiometric Performance

The inflight radiometric calibration accuracy and the stability thereof are pivotal for realizing high-precision measurements of global atmospheric CO_2 concentrations [15]. In this

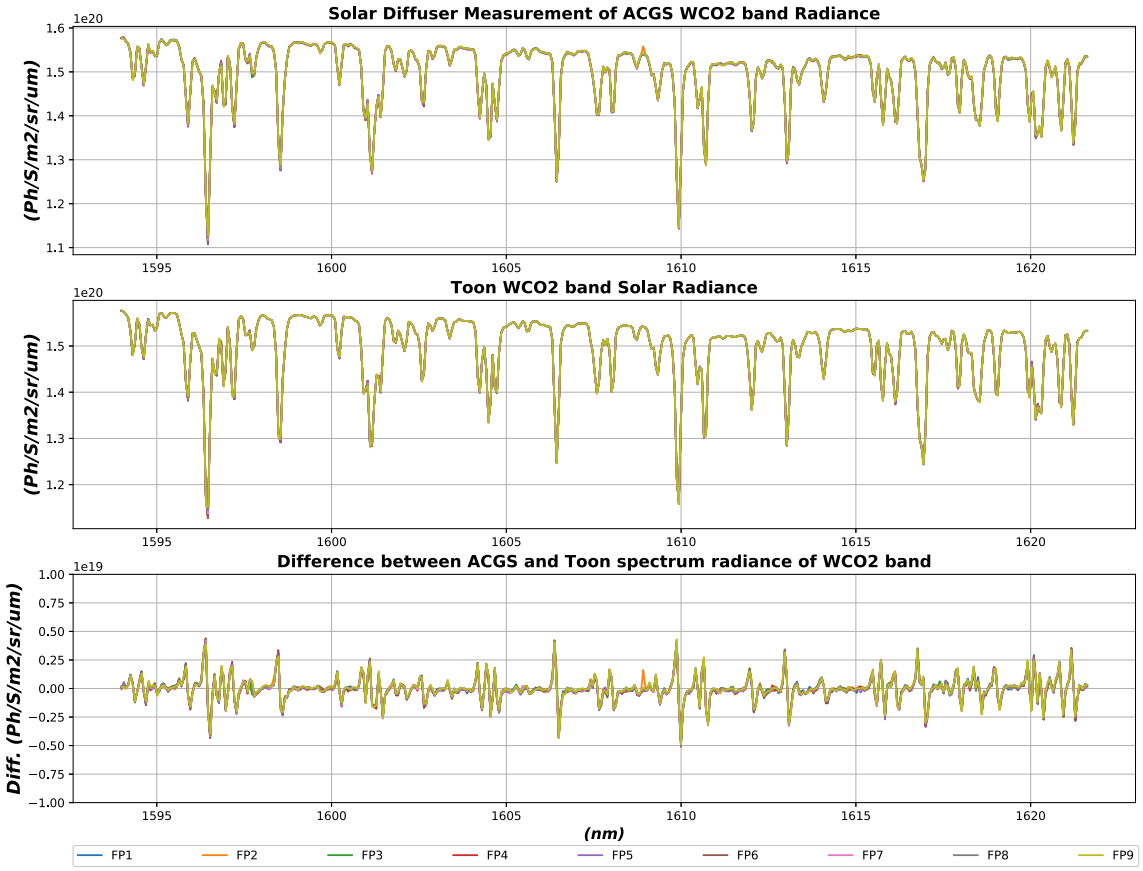

Fig. 4. Inflight spectroscopic performance of the ACGS WCO_2 band in nine footprints.

section, we evaluate the inflight radiometric performance, including the dark current response, SNR, and gain coefficient. We analyze the total uncertainty of the radiometric calibration and present the inflight radiometric calibration results.

1) Dark Current: Dark current refers to the response of an instrument detector when it is not actively being irradiated. For the HgCdTe detectors of the WCO_2 and SCO_2 bands of the ACGS, the response component is sensitive to minuscule changes in the ambient temperature, although the temperature is controlled to be within 0.3 K inflight, and thus, it must be corrected routinely inflight. Preliminary dark current responses as a function of the ambient temperature were established for the two CO_2 bands during the thermal-vacuum (TVAC) testing of the ACGS [11].

The dark current model in this work is based on two assumptions: first, the dark current of the FPA of the two CO_2 bands is a response to the ambient temperature, and second, the response of each detector of a tiny FPA is similar. Thus, we can use the Dn of the shielded margin pixels to estimate the dark current of the unshielded pixels for each spectral channel in different observation modes because they have very good linear relationships. The prelaunch TVAC testing of the ACGS demonstrated that these two assumptions are true. Because the TVAC could not perfectly simulate the environmental heat fluxes found in the real orbit, we reestablished the dark model for each spectral channel in the different observation modes inflight when the ACGS powered on and the shutter closed; this function is a special design of the ACGS. The experiment of the inflight dark current of the ACGS continues for a few days, and the measurement data from dozens of orbits in different observation modes can be obtained. We used only 75% of the data to establish the dark current model and used the other 25% to verify this model. The verified results show that the accuracy of the model is better than 10–15 Dn.

Each shielded margin pixel consists of 16 array elements on the FPA, and each unshielded middle pixel (spectral channel) consists of 12 array elements on the FPA. Because the illuminated pixels and shielded pixels consist of different numbers of detector elements and have slightly different readout circuits, the precise number of DNs is not expected to match between the two-pixel types. However, the very good linear relationship shown in Fig. 7 across the three observation modes shows that the linear model can be used to predict the dark current in the illuminated pixels using the shielded pixels' values. The left panel is the WCO_2 band, and the right panel is the SCO_2 band. These models have been used to estimate the dark current of the ACGS in the preprocessing algorithm of the L1 products, and the performance has been validated in our X_{CO_2} retrieval processing. After the corrections were used in these models, the dark current error was below 15 counts in the two CO_2 bands of the ACGS.

The O_2 A-band uses a Si detector with a dark current response of tens of counts, and this result varies by only between 2 and 3 counts during a full-orbit dark current

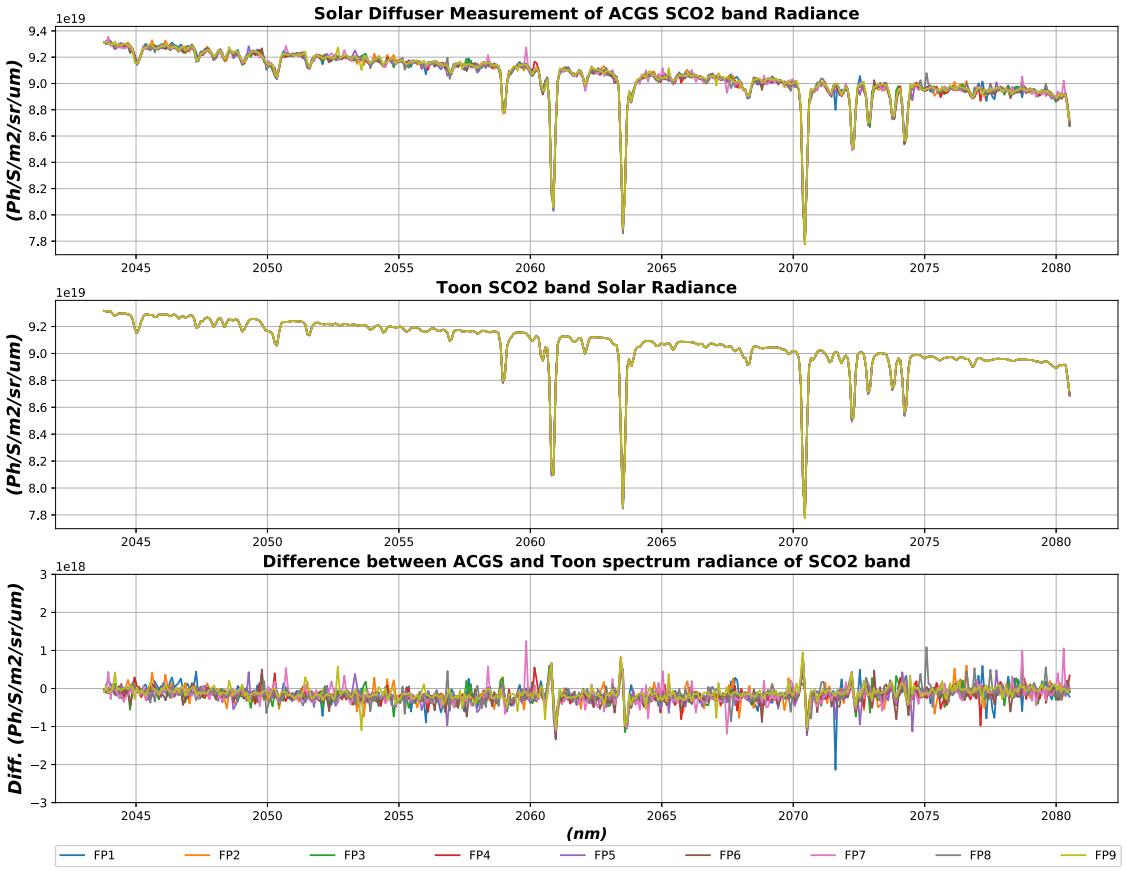

Fig. 5. Inflight spectroscopic performance of the ACGS SCO_2 band in nine footprints.

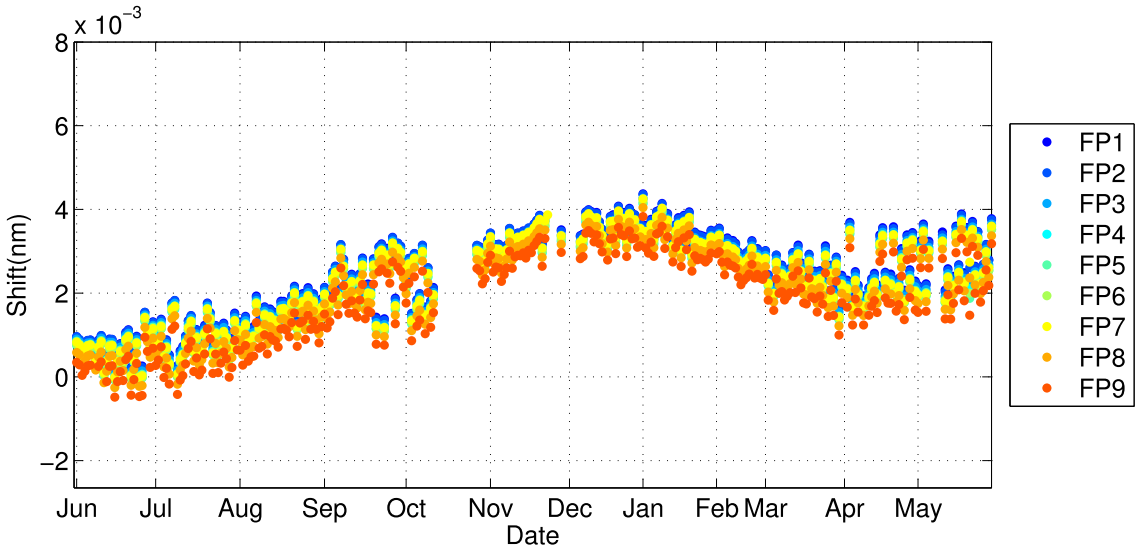

Fig. 6. Stability of the spectral accuracy in the O2 A-band over a year from June 2017 to May 2018.

calibration, indicating that this test exhibits a minimal temperature sensitivity. Because the ambient temperature is controlled to be within 0.3 K inflight, this sensitivity should be negligible inflight.

2) SNR: SNR is a measurement that compares the level of the desired signal to the level of background noise; that is, SNR measures the ratio between an arbitrary signal level and that of the noise. Measuring SNR requires the selection of a reference signal source. In the prelaunch calibration of the ACGS, we used a National Institute of Standards and Technology (NIST)-traceable integrating sphere as the reference signal source to successfully characterize the SNR [11]. In-flight, we used measurements of the calibration lamp devices and solar diffuser to evaluate the SNR of the ACGS

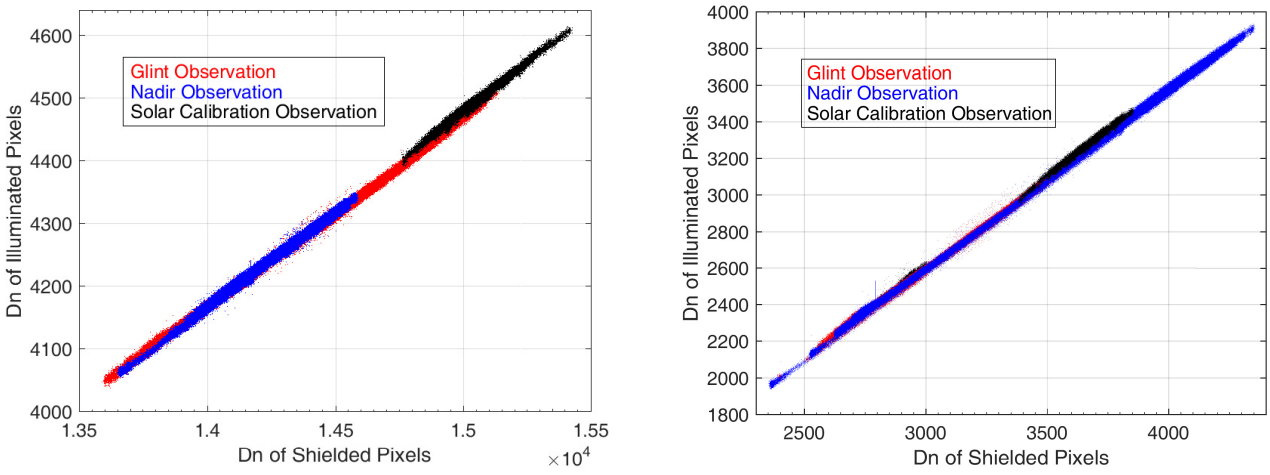

Fig. 7. Inflight dark current response model of (a) WCO_2 band footprint 9 channel 250 and (b) SCO_2 band footprint 9 channel 250.

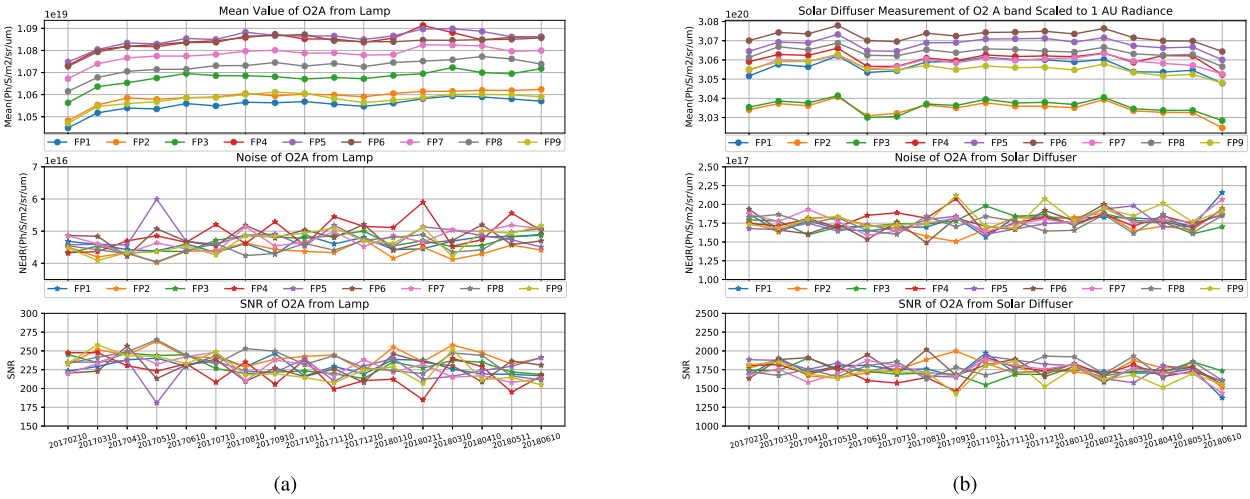

Fig. 8. Inflight performance stability of O_2 A-band channel 622 in nine footprints. (a) Calibration lamp. (b) Solar diffuser.

using formulas (1)–(3). In this article, the SNR is defined as the ratio of the mean to the standard deviation of a measured signal.

$$\mu = \frac{1}{n}\sum_{i=1}^{n} x_i \tag{1}$$

$$\sigma = \sqrt{\frac{1}{n-1}\sum_{i=1}^{n}(x_i - \mu)^2} \tag{2}$$

$$\text{SNR} = \frac{\mu}{\sigma} \tag{3}$$

where x is a sample of the measured radiance from a calibration lamp or solar diffuser, n is the sample size of the radiance measurements (n equals 180 in this article), μ is the mean of the measured values (also called the mean value in statistical science and this article), and σ is the noise, computed as the standard deviation of the measured radiance that is defined as the noise-equivalent differential radiance (NEdR) in this article. Thus, the noise is a critical indicator for the inflight performance of the ACGS.

Figs. 8–10 show the time series of the mean values, noise, and SNR of one channel randomly selected from the three bands. All of these measurements represent pivotal inflight performance metrics for the ACGS. The time series range from the time at which the instrument was powered on to the time of writing this article. These raw data come from measurements of the inflight calibration lamp and solar diffuser.

Fig. 8 shows the time series of the mean values, noise, and SNR of O_2 A-band channel 622 in all nine footprints ranging from February 10, 2017 to June 10, 2018, representing the statistical results of 180 samples in one minute on the tenth day of each month. The results in the left column come from calibration lamp measurements; the upper-left panel shows the mean values, the middle-left panel displays the noise, and the bottom-left panel illustrates the SNR. The results on the right column originate from solar diffuser measurements; the upper-right panel shows the mean values scaled to 1 AU Earth–Sun distance, the middle-right panel

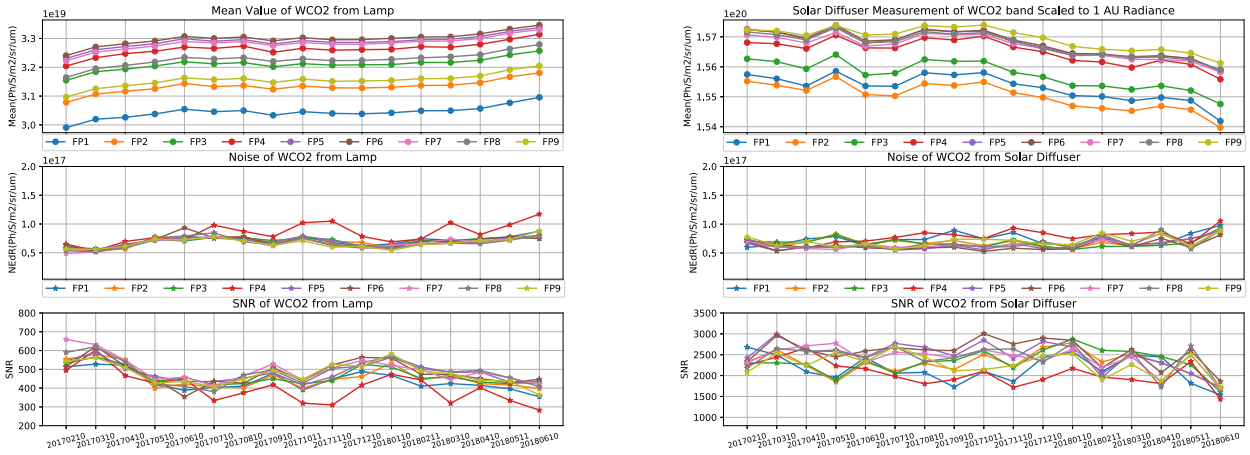

(a) (b)

Fig. 9. Inflight performance stability of WCO_2 band channel 251 in nine footprints. (a) Calibration lamp. (b) Solar diffuser.

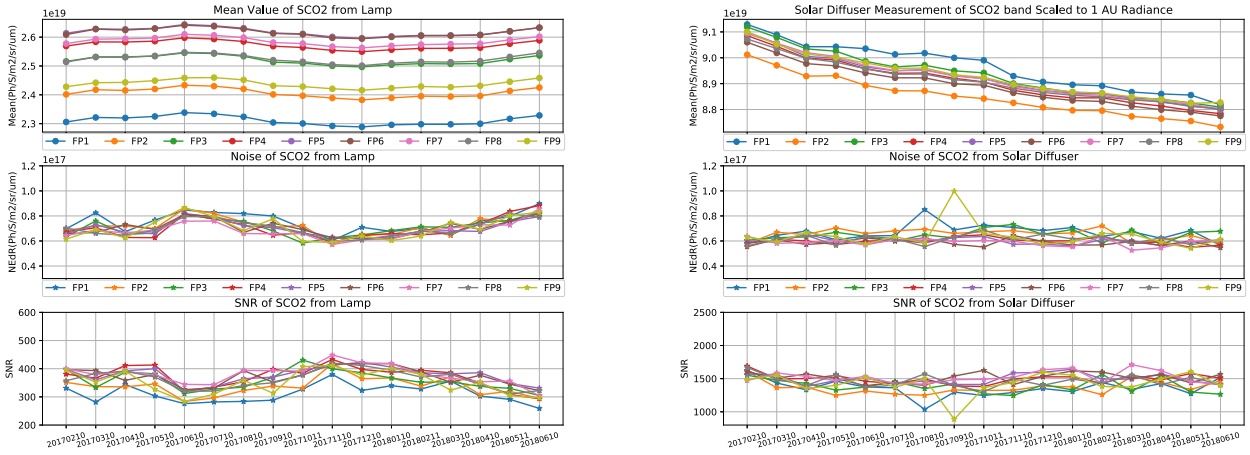

(a) (b)

Fig. 10. Inflight performance stability of SCO_2 band channel 252 in nine footprints. (a) Calibration lamp. (b) Solar diffuser.

displays the noise, and the bottom-right panel illustrates the SNR. The different colors in these figures represent nine footprints. Figs. 9 and 10 are configured with the same pattern as Fig. 8. The calibration lamp measurements on the left column of Fig. 8 illustrate the significant stability of the time series during the past 16 months. The mean value remains at 1.04e + 19∼1.08e + 19 (photons/s/m_2/sr/μm) in the nine footprints, and the differences between each footprint are very small (∼1.5%). The noise-equivalent radiance levels remain at ∼0.5e + 17 (photons/s/m_2/sr/μm) in the nine footprints and are particularly stable. The SNR values of O_2 A-band channel 622 in all nine footprints during the lamp measurements remain at 200–250, thereby meeting the mission requirements.

The measurements from the solar diffuser scaled to 1 AU Earth–Sun distance on the right column of Fig. 8 display very good stability (also shown in Figs. 9 and 10). The uncertainty of the O_2 A-band channel 622 is better than ∼0.5%. The noise-equivalent radiance levels from the solar diffuser measurements remain at 1.5e + 17∼2.0e + 17 (photons/s/m_2/sr/μm) in the nine footprints, and the values show clear stability.

Figs. 9 and 10 show the time series of the mean values, noise, and SNR of WCO_2 band channel 251 and SCO_2 band channel 252 in all nine footprints during the same period. Correcting for the variation in the solar intensity due to variations in the Sun–Earth distance, the uncertainty of the WCO_2 bands is better than 0.24%, and that of the SCO_2 bands is better than 3.03%. These results demonstrate more remarkable consistency among the nine footprints from the two types of measurements, namely, lamp and solar diffuser measurements. In addition, the measured solar diffuser mean value in Fig. 10 shows a ∼3.0% degradation in the SCO_2 band during the first 16 months but a normal lamp measurement in the SCO_2 band. This finding may suggest that the solar diffuser was declining in the SCO_2 band. The noise-equivalent radiance levels from different order-of-magnitude measurements from the lamp and solar diffuser present similar values of ∼0.6e + 17(photons/s/m_2/sr/μm), indicating that the noise is

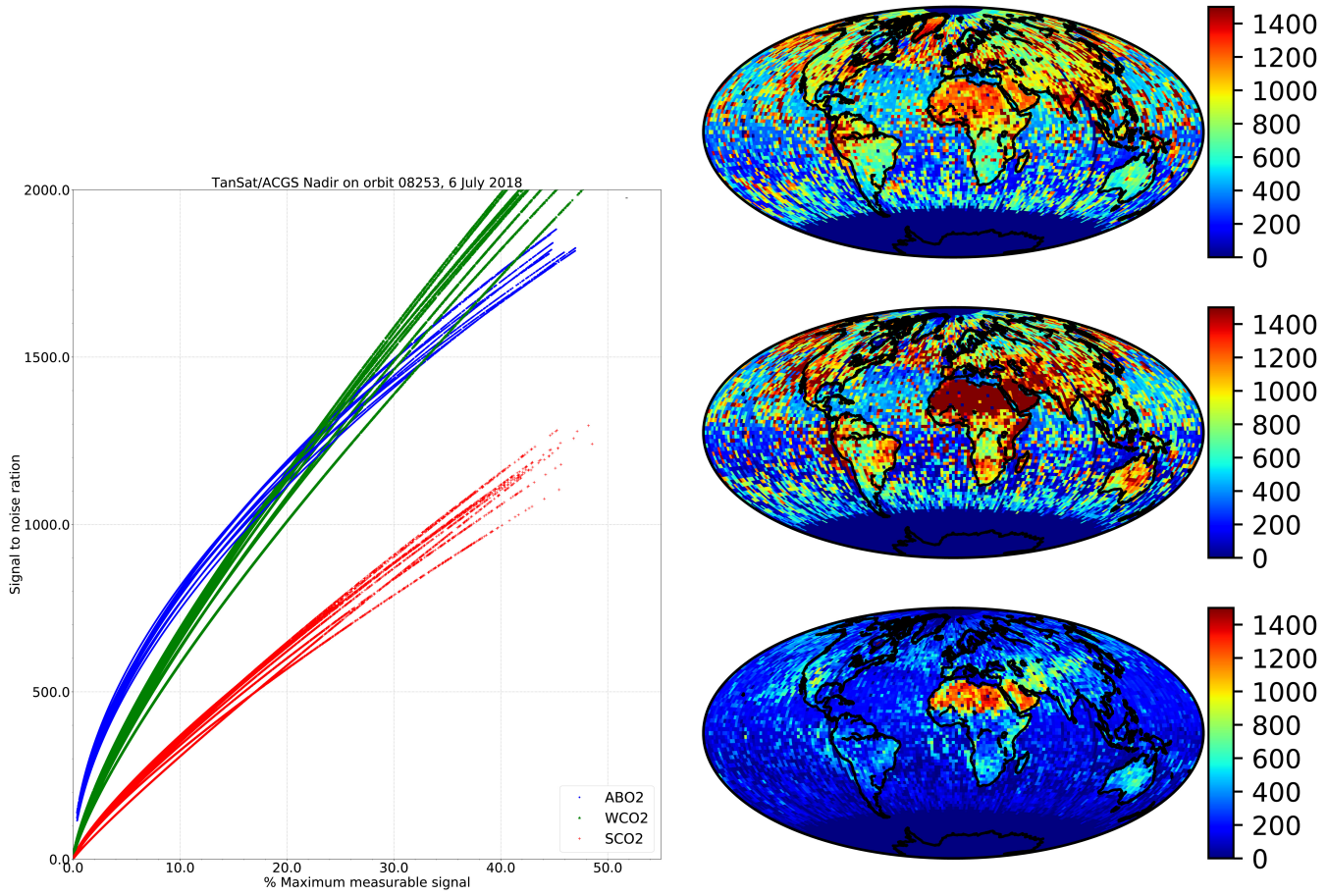

(a) (b)

Fig. 11. (a) SNRs for individual soundings in the O_2A (blue line), WCO_2 (green line), and SCO_2 (red line) bands are shown as a function of the percent maximum measurable signal for a nadir orbit observed on July 6, 2018. The parallel traces show results for the night footprints in each channel. (b) Mean continuum single-sounding SNRs global map in $2^\circ \times 2^\circ$ bins for the O_2A (top), WCO_2 (green line) (middle), and SCO_2 (bottom) bands in July 2018.

independent and demonstrates satisfactory stability. The SNR values of WCO_2 band channel 251 and SCO_2 band channel 252 in all nine footprints of the lamp measurements remained near 400–600 and 300–450, respectively, thereby meeting the mission requirements.

The radiometric calibration of the ACGS was accomplished prelaunch through two calibration measurements of a calibrated integrating sphere with reference radiometers validated against NIST (see [11], [12]). These tests indicated that the SNRs of all three bands met the mission requirements. The SNRs of individual spectral sample channels recorded during a typical nadir orbit are shown in Fig. 11 (left). The SNRs for individual sounding inflight come from the SNR model established during prelaunch laboratory measurements (see [11]). In this example, the intensities in the O_2 A (blue line), WCO_2 (green line), and SCO_2 (red line) bands spanned ~48% of their maximum measurable signals. Global maps of the continuum SNR in nadir science observation for July 2018 are shown in Fig. 11 (right). In this figure, the mean continuum SNR values for each channel have been averaged into $2^\circ \times 2^\circ$ bins. The largest SNR values are generally recorded over the Sahara, the Middle East, and Australian deserts, which are very similar to the results of OCO2 (see [3]).

3) Gain Coefficient: The gain coefficient of the radiometric calibration is a pivotal performance metric for characterizing the response characteristics of the ACGS and is used to convert the measured DN (digital number) into the spectral radiance. In Figs. 3–5 and 8–10, we converted raw measured DNs (dimensionless) into spectral radiance data (photons/s/m_2/sr/μm) by the prelaunch gain coefficients of the three ACGS bands.

We use the solar reference spectra as a benchmark to evaluate the inflight radiometric calibration accuracy of the ACGS. The solar continuum model that we used is the same as that of OCO-2, which is based on a polynomial fit to the NIR part of the low-resolution extraterrestrial solar spectrum acquired by the Solar Spectrum (SOLSPEC) instrument [16]. The uncertainty of the SOLSPEC data is estimated to be 1% and 3% when the wavelength is less than 2500 nm and when the wavelength is close to 2500 nm, respectively. We assume that the solar continuum is invariant over time. According to the results of prelaunch laboratory measurements, the BRDF uncertainty of the solar diffuse reflector of the ACGS is less than 1.5% and 1.9% for the O_2 A-band and two CO_2 bands, respectively [11]. The Sun fully illuminates the spectral samples of the ACGS during calibration. The front of the

TABLE II
INFLIGHT CALIBRATION TECHNIQUES AND COMPARISON OF ACGS'S PERFORMANCES BETWEEN PRELAUNCH AND INFLIGHT

Item	Band	Prelaunch	Inflight	Techniques in-flight
Wavelength position calibration (Bias/RMS)(pm)	O_2A	∼/0.9	+2.93/0.19	Solar measurements with reference Fraunhofer line spectrum.
	WCO_2	∼/1.0	-42.9/0.27	
	SCO_2	∼/0.7	-46.7/4.75	
Absolute Radiometry (%)	O_2A	4.45	3.81	Solar measurements using Thuillier SOLSPEC reference continuum.
	WCO_2	4.58	3.04	
	SCO_2	4.61	4.53	
Radiometric calibration stability over time (%/yr)	O_2A	1.50 (0.5 yr)	L:0.35 S:0.08	Solar and Lamp measurements.
	WCO_2	1.55 (0.5 yr)	L:0.56 S:0.17	
	SCO_2	2.10(0.5yr)	L:0.41 S:2.13	

pointing mechanism of the ACGS is the mirror, and the back is the diffuse reflector. The front side of the pointing mechanism reflects the Earth-atmospheric radiation into the focal telescope of the ACGS during the Earth-view observation, while the diffuse reflector of the back side also reflects solar irradiation into the focal telescope during the solar calibration. Thus, they share the same optical path from the telescopes to FPAs. In sum, it is feasible to use this method to evaluate the accuracy of the radiometric calibration.

From the differences between the spectral radiance of the solar calibration and the solar reference spectra of one observation in Figs. 3–5, we estimated that the percentage of the differences of the O_2 A-band, the WCO_2 band, and the SCO_2 band is less than 3.7%, 2.8%, and 1.5%, respectively. Using the 17-month inflight calibration data in Figs. 8–10, we calculated the uncertainty of the O_2 A-band to be better than 0.11%, that of the WCO_2 band to be better than 0.24%, and that of the SCO_2 band to be better than 3.03%. Based on the analysis of the above two types of results, the radiometric calibration accuracy should be the sum of the two results; that of the O A-band, the WCO_2 band, and the SCO_2 band is 3.81%, 3.04%, and 4.53%, respectively, and they all met the mission requirement of 5%.

IV. RESULTS AND DISCUSSION

The performance parameters of the ACGS in previous work [11], [12] using prelaunch laboratory testing indicated that the dark current, SNR, spectral resolution and resolving, and radiometric calibration met the mission requirements. In this article, we used inflight solar diffuser reflector and lamp calibration data to evaluate the inflight performance of the ACGS. The lamp data were used to monitor the stability of the radiometric response, while the data of the solar diffuse reflector were used to evaluate the accuracy and stability of the wavelength and radiometric calibration. The evaluation results were compared with prelaunch laboratory test data. Table II shows these comparison results.

The stability of the ACGS performance is very important for using its measurements to estimate atmospheric CO_2 concentrations. In this article, we used the coefficient of variation (CV) as the stability index, also called uncertainty. The CV is a statistical measure of the dispersion of data points in a data series around the mean and is the ratio of the standard deviation to the mean. Using 17 months of solar diffuse reflector calibration data during February 2017–June 2018, we calculated the stability of the O_2 A-band to be better than 0.11%, that of the WCO_2 band to be better than 0.24%, and that of the SCO_2 band to be better than 3.03%. We scale the stability of 17 months to per year numbers, which are 0.08%, 0.17%, and 2.13% of the O2-A, WCO_2, and SCO_2 bands. Using the 17 months of lamp data, we calculated the stability per year of the O_2 A-band to be better than 0.35%, that of the WCO_2 band to be better than 0.56%, and that of the SCO_2 band to be better than 0.41%.

In the prelaunch laboratory testing, the stability of the ACGS performance was the difference between two independent tests taken during a half year. As shown in Table II, the response stability of the ACGS inflight is better than that prelaunch from both the lamp and solar diffuse reflector; the values are better than 0.79% (17 months), except for that of the SCO_2 band. We believe that the results inflight are more reliable because the ambient conditions inflight are more consistent than those between the two laboratory tests. Another item, the dark current, shows a similar result. The dark current of the O_2 A-band is the same prelaunch and inflight because it is independent of the ambient temperature, while the dark current inflight of the two CO_2 bands is less than that prelaunch. Other performance metrics, such as the noise, signal level, radiometric calibration, and wavelength calibration, in-flight are in line with the results of the prelaunch laboratory testing.

The results of the response stability of the SCO_2 band in Table II and Fig. 10 indicate that the radiometric response in the SCO_2 band appears to be decaying during the 17 months. However, at the same time, the radiometric response in the SCO_2 band of the lamp calibration is very stable (0.58%/17 months). Thus, we cannot confirm that this is a problem with the response of the ACGS itself because it may be an issue with the diffuse reflector, which needs to be investigated further. Nevertheless, the results in Table II suggest that the measurement of the ACGS inflight can provide reliable information for estimating the atmospheric CO_2 concentration.

V. CONCLUSION

Many prior works have documented the critical importance of validating the inflight radiometric and spectroscopic

accuracies of a sensor for retrieving valuable atmospheric XCO_2 [3], [9], [10]. These data have been used in atmospheric chemistry transport models to quantify the surface sources and sinks of CO_2 and to support global warming research [6], [7], [17]. Prelaunch calibration and validation investigations successfully established a baseline of the instrument characterization and performance, as well as the initial set of instrument calibration coefficients and parameters for inflight L1 processing [11], [12]. In this article, we evaluated the inflight spectroscopic and radiometric performance of the ACGS using data measured from the solar diffuser and halogen tungsten lamp devices. To date, inflight calibration and validation work has achieved success, and the radiometric and spectral performance specifications have met the mission requirements.

The inflight performance of the ACGS can be summarized as follows. The wavelength calibration accuracy of the O_2 A-band is $\sim$0.19 pm, that of the WCO_2 band is $\sim$0.27 pm, and that of the SCO_2 band is $\sim$4.75 pm after bias correction, all of which meet the 0.05 FWHM requirement. The spectroscopic performance of the ACGS surpasses the mission requirements by a margin. The inflight dark current error was below 15 counts in the two CO_2 bands of the ACGS. Based on the analysis of the two types of results in the previous section, the radiometric calibration accuracy should be the sum of the two results; that of the O A-band, the WCO_2 band and the SCO_2 band is 3.81%, 3.04%, and 4.53%, respectively, and they all met the mission requirement of 5%. The ACGS possesses comparable or smaller noise levels than those measured during prelaunch testing, as demonstrated in Figs. 8–10, and the noise level has remained stable in the three bands during inflight operations. The SNRs of the three bands thus meet the specified requirements. As expected, at the time of this writing, the ACGS radiometric performance in the O_2 A-band and in the WCO_2 and SCO_2 bands was acceptable.

Since the ACGS instrument was powered on in early February 2017, a well-planned series of calibration and validation activities have been performed with the goal of providing well-calibrated and characterized L1 products. On October 24, 2017, we released the Ver 1.0 L1 products to the world. Subsequently, Ver 2.0 L1 products were released to the world on February 1, 2018 (http://satellite.nsmc.org.cn/portalsite/default.aspx). The estimated absolute spectral calibration uncertainty is less than one-tenth of the spectral resolution, and the estimated radiometric uncertainty is less than 5% in the O_2 A-band and WCO_2 and SCO_2 bands. In February 2018, the NSMC TanSat team completed the research and software development phase of a full physical inversion algorithm for X_{CO_2}. The software has since been placed into operation, the initial accuracy verification has been completed, and large-scale batch processing and validation efforts are underway.

ACKNOWLEDGMENT

The authors would like to thank all the members of the TanSat Team, including the employees of NSMC, CIOFMP, and SECM who worked wisely and tirelessly in acquiring and processing the ACGS inflight data. The research described in this article was carried out at NSMC through a major project of the Ministry of Science and Technology (MOST) of the China Earth Observation Program under Contract 2011AA12A104. Although every effort has been made to ensure that the contents of this article are accurate, any mistakes are the responsibility of the authors. They would also like to thank two anonymous reviewers for their thoughtful comments on the original manuscript.

REFERENCES

[1] "WMO greenhouse gas bulletin 2017," Atmos. Environ. Res. Division, Res. Dept., World Meteorol. Org., Geneva, Switzerland, Tech. Rep., 2017.

[2] M. Gottwald and H. Bovensmann, *SCIAMACHY—Exploring the Changing Earth's Atmosphere*. London, U.K.: Springer, 2011.

[3] D. Crisp *et al.*, "The on-orbit performance of the Orbiting Carbon Observatory-2 (OCO-2) instrument and its radiometrically calibrated products," *Atmos. Meas. Tech.*, vol. 10, no. 1, pp. 59–81, Jan. 2017. [Online]. Available: http://www.atmos-meas-tech-discuss.net/amt-2016-281/

[4] A. Eldering *et al.*, "The Orbiting Carbon Observatory-2: First 18 months of science data products," *Atmos. Meas. Techn.*, vol. 10, no. 2, pp. 549–563, 2017.

[5] F. Sakuma *et al.*, "OCO/GOSAT preflight cross-calibration experiment," *IEEE Trans. Geosci. Remote Sens.*, vol. 48, no. 1, pp. 585–599, Jan. 2010.

[6] A. Agusti-Panareda, M. Diamantakis, V. Bayona, F. Klappenbach, and A. Butz, "Improving the inter-hemispheric gradient of total column atmospheric CO_2 and CH_4 in simulations with the ECMWF semi-Lagrangian atmospheric global model," *Geosci. Model Develop.*, vol. 10, no. 1, pp. 1–18, Jan. 2017.

[7] B. Byrne, D. B. A. Jones, K. Strong, Z.-C. Zeng, F. Deng, and J. Liu, "Sensitivity of CO2 surface flux constraints to observational coverage," *J. Geophys. Res., Atmos.*, vol. 122, no. 12, pp. 6672–6694, Jun. 2017.

[8] C. E. Miller *et al.*, "Precision requirements for space-based data," *J. Geophys. Res., Atmos.*, vol. 112, no. 10, pp. 1–19, 2007.

[9] F. Chevallier, G. Broquet, C. Pierangelo, and D. Crisp, "Probabilistic global maps of the CO 2 column at daily and monthly scales from sparse satellite measurements," *J. Geophys. Res. Atmos.*, vol. 122, no. 14, pp. 7614–7629, Jul. 2017.

[10] D. M. Hammerling, A. M. Michalak, and S. R. Kawa, "Mapping of CO_2 at high spatiotemporal resolution using satellite observations: Global distributions from OCO-2," *J. Geophys. Res., Atmos.*, vol. 117, no. 6, 2012.

[11] Z. Yang *et al.*, "Prelaunch radiometric calibration of the TanSat atmospheric carbon dioxide grating spectrometer," *IEEE Trans. Geosci. Remote Sens.*, vol. 56, no. 7, pp. 4225–4233, Jul. 2018.

[12] Z. Yang *et al.*, "Laboratory spectral calibration of the TanSat atmospheric carbon dioxide grating spectrometer," *Geosci. Instrum. Method. Data Syst.*, vol. 7, no. 3, pp. 245–252, Aug. 2018. [Online]. Available: https://www.geosci-instrum-method-data-syst.net/7/245/2018/

[13] D. Crisp, L. Brown, J. Mcduffie, C. O. Dell, D. O. Brien, and D. Thompson, "OCO (Orbiting Carbon Observatory)-2 level 2 full physics retrieval algorithm theoretical basis," Jet Propuls. Lab., California Inst. Technol., Pasadena, CA, USA, Tech. Rep. Version 2.0 Rev. 2, Data Releases 6 and 6R, Mar. 2015.

[14] K. Sun *et al.*, "Characterization of the OCO-2 instrument line shape functions using on-orbit solar measurements," *Atmos. Meas. Tech.*, vol. 10, no. 3, pp. 939–953, Mar. 2017.

[15] B. Connor *et al.*, "Quantification of uncertainties in OCO-2 measurements of XCO2: Simulations and linear error analysis," *Atmos. Meas. Tech.*, vol. 9, no. 10, pp. 5227–5238, Oct. 2016.

[16] G. Thuillier *et al.*, "The solar spectral irradiance from 200 to 2400 nm as measured by the SOLSPEC spectrometer from the Atlas and Eureca missions," *Sol. Phys.*, vol. 214, no. 1, pp. 1–22, 2003.

[17] P. Rayner, A. M. Michalak, and F. Chevallier, "Fundamentals of data assimilation," *Geosci. Model Develop. Discussions*, pp. 1–21, Jul. 2016. [Online]. Available: http://www.geosci-model-dev-discuss.net/gmd-2016-148/

Zhongdong Yang received the B.S. and M.S. degrees from the Xinjing University, Xinjiang, China, in 1987 and 1990, respectively, and the Ph.D. degree in remote sensing science from the Institute of Geology, Beijing, China, in 1997.

He is currently a Senior Scientist with the National Satellite Meteorological Center (NSMC), Chinese Meteorological Administration, Beijing. Since 2010, he has worked as the Chief Scientist of the Ground Segment Project of the FY-3 meteorological satellite series. He is also the Chief Scientist of the TanSat Ground Segment Project and plays a leading role in the data processing, algorithm development, and ground segment projects of the FY-3 satellites and TanSat.

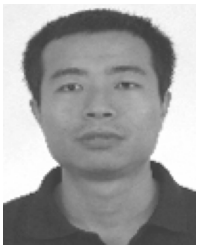

Yan-Meng Bi received the Ph.D. degree in atmospheric physics science from the Peking University, Beijing, China, in 2003.

He is currently a member of the TanSat Team at the National Satellite Meteorological Center (NSMC), Beijing, where he is responsible for the preprocessing of TanSat data. His research interest is in the remote sensing of CO_2 from satellites.

Qian Wang received the M.S. degree from the Chinese Academy of Meteorological Sciences, Beijing, China, in 2014.

She is currently a member of the TanSat Team at the National Satellite Meteorological Center (NSMC), Beijing. Her research interest is in the remote sensing of the atmospheric composition from satellites.

Cheng-Bao Liu received the Ph.D. degree in applied mathematics from the University of Chinese Academy of Sciences, Beijing, China, in 2013.

He is currently researching a geolocation algorithm for remote sensing data from the FengYun meteorological satellites at the National Satellite Meterological Center of CMA, Beijing. His major contribution to the TanSat Mission is providing geolocation information for satellite remote sensing data.

Song-Yan Gu received the Ph.D. degree from Peking University, Beijing, China.

She is currently the Deputy Chief Designer of the FY-3 satellite and a member of the TanSat Team at the National Satellite Meteorological Center (NSMC), Beijing, where she is responsible for the preprocessing of TanSat data.

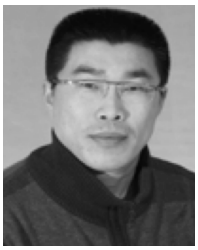

Yuquan Zheng received the Ph.D. degree in optical science from the Changchun Institute of Optics, Fine Mechanics and Physics, Chinese Academy of Sciences, Changchun, China, in 1999.

He is currently a Senior Research Scientist and the Director of the Space Optics Department, Changchun Institute of Optics, Fine Mechanics and Physics, where he was a Deputy Project Scientist for the TanSat mission and served as the Project Manager for the ACGS.

Chao Lin received the M.S. degree in mechanical engineering from the Jilin University, Changchun, China, in 2009.

He is currently an Assistant Scientist with the Space Optics Department, Changchun Institute of Optics, Fine Mechanics and Physics, where he was a Deputy Project Lead for the TanSat ACGS and was mainly in charge of the spectral and radiometric calibration of the ACGS.

Zengshan Yin received the Ph.D. degree from Zhejiang University, Hangzhou, China.

He is currently a Professor and a Chief TanSat Platform Designer with the Shanghai Engineering Centre for Microsatellites, Chinese Academy of Sciences, Shanghai, China. He has been selected as an expert on the remote sensing satellites of China. His main research interest is in satellite system design.

Longfei Tian received the M.S. degree from Northwestern Polytechnical University, Fremont, CA, USA.

He is a Designer of TanSat with the Shanghai Engineering Centre for Microsatellites, Chinese Academy of Sciences, Shanghai, China. His main research interest is in satellite system design.